Desalination and Water Treatment
www.deswater.com

doi: 10.5004/dwt.2019.23100

143 (2019) 240–255
March

Adsorption optimization of Cr(VI) and Co(II) onto the synthesized chitosan/cerium oxide/iron oxide nano-composite in water system using RSM according to CCD method

Morshed Farokhi[a], Arsalan Parvareh[a,b,*], Mostafa Keshavarz Moraveji[a,c]

[a]*Department of Chemical Engineering, Borujerd Branch, Islamic Azad University, Borujerd, Iran, email: Morshed_Farokhi@yahoo.com*
[b]*Chemical Engineering and Petroleum Faculty, Razi University, Kermanshah, Iran, Tel. +98 831 4274530; Fax: +98 831 4274542; email: A.parvareh@razi.ac.ir (A. Parvareh)*
[c]*Department of Chemical Engineering, Amirkabir University of Technology (Tehran Polytechnic), 242 Hafez Avenue, Tehran 15875-4413, Iran, email: Moraveji@aut.ac.ir (M.K. Moraveji)*

Received 18 March 2018; Accepted 1 September 2018

ABSTRACT

The chitosan/cerium oxide/iron oxide (chitosan/CeO_2/Fe_3O_4) nano-composite adsorbent was synthesized for the removal of Cr(VI) and Co(II) ions from aqueous solution in a batch system. The adsorbents were characterized by field emission scanning electron microscopy, transmission electron microscopy, Fourier transform infrared spectroscopy, Brunauer–Emmett–Teller and X-ray diffraction analyses. The effect of CeO_2 and Fe_3O_4 contents on the adsorption capacity was studied. The adsorption capacity was significantly increased after modification of adsorbents with CeO_2 and Fe_3O_4 nanoparticles. Furthermore, the simultaneous effects of four independent variables including initial metal concentration, temperature, solution pH and adsorbent dosage were studied using response surface methodology. The optimum adsorption capacity was found to be 208.18 and 172.92 mg/g for Cr(VI) and Co(II) ions, respectively, under the following adsorption conditions: initial concentration of 200 mg/L, temperature of 20°C, adsorbent dosage of 10 mg, initial pH 5.54 for Cr(VI) and pH 9.00 for Co(II) ions. The validation tests showed that the predicted model agreed well with the adsorption experimental data. The isotherm and kinetic data were precisely described by the Langmuir and pseudo-second-order models, respectively. The maximum adsorption capacity obtained from Langmuir isotherm were 316.10 and 263.57 mg/g for Cr(VI) and Co(II) ions, respectively. Thermodynamic investigation showed that the nature of adsorption process was exothermic and spontaneous.

Keywords: Chitosan/cerium oxide/iron oxide nano-composite; Cr(VI) and Co(II) sorption; Response surface methodology; Isotherm models; Central composite design

1. Introduction

In general, the pollutants such as heavy metals, dyes, hydrocarbons lead to a risk for environment and human health [1–5]. The pollutions in the environment originate from mining, metallurgical, painting, battery manufacture, fertilizing and tanning [6–8]. Chromium and cobalt indicated the genotoxic effects and they are the common toxic pollutants affecting the human health and living creatures [9–12]. The Cr(VI) and Co(II) are toxic carcinogenic ions which get readily absorbed into the body [13]. Also, they can lead to several health problems including low blood pressure, diarrhea, bone defects and lung irritation [13,14]. Thus, it is necessary to develop the effective methods for elimination of these toxic metals from water systems. Nowadays, many methods have been applied for the removal of toxic metals containing electrocoagulation [15], evaporation [16], membrane process [7], flotation [17], solvent extraction

* Corresponding author.

[18] and precipitation [19]. The methods mentioned above usually need high energy consumption leading to the high costs for high volumes of polluted water and also are not effective at very dilute solutions [20]. Adsorption process is an effective method for the removal of heavy metals from water systems [21–25]. Furthermore, the adsorption process has promising advantages including high adsorption efficiency, simple adsorbent regeneration and easy operations [26,27]. On the other hand, the type of adsorbent is a serious issue in the adsorption process. The various adsorbents have been evaluated for the removal of heavy metal ions from water systems. Nano-sized metal oxides such as cerium oxide and iron oxides were useful adsorbents due to their high surface areas, small sizes, high electric charges and surface reaction sites [28–32]. Electrostatic attraction and ligand exchange of heavy metal ions with metal oxides are possible mechanisms for adsorption process [11,33]. For instance, the protonated surface of nano iron oxide impregnated in chitosan bead including Fe–OH_2^+ and NH_3^+ (both in composite) attracts the anionic Cr(VI) species by electrostatic attraction mechanism. Furthermore, the ligand exchange Fe–OH groups in the nano-composite structure with anionic Cr(VI) species is another adsorption mechanism [11]. Nevertheless, instability of nano-sized metal oxides in water systems (in powder forms) is one of the most important limitations leading to the agglomeration of nanoparticles in the solution owing to the several interactions and van der Waals forces [34]. Thus, this unstable state reduces the surface area, mechanical strength and adsorption capacity [34]. Also, the separation and filtration of nano-sized metal oxides is very difficult after adsorption process [35]. To overcome these limitations, the nano-sized metal oxides composed with a matrix-like polymers [11]. Between the polymers, chitosan is a practicable adsorbent due to its environmental compatibility, low cost and its functional groups such as $–NH_2$ and –OH groups which has appropriate potential for high adsorption of heavy metal ions from water systems [11,36,37]. Therefore chitosan/metal oxide nano-composites are effective adsorbents because of their high resistance in water solution, high adsorption efficiency and their low-cost synthesis process [38]. Consequently, the combination of metal oxides (CeO_2 and Fe_3O_4) and chitosan adsorbents is promising and beneficial to bond Cr(VI) and Co(II) ions because these nano-composites have multifunctional groups for adsorption process. Up to now, the composites of cerium oxide/iron oxide based on chitosan with multifunctional groups have not been synthesized for the adsorption of heavy metal ions from aqueous solutions.

In this research, the main objective was the synthesis of the novel chitosan/CeO_2/Fe_3O_4 nano-composites as potential adsorbents for the removal of Cr(VI) and Co(II) ions from aqueous solutions. The nano-composite adsorbents were characterized by field emission scanning electron microscopy (FESEM), transmission electron microscopy (TEM), Fourier transform infrared spectroscopy (FTIR), Brunauer–Emmett–Teller (BET) and X-ray diffraction (XRD) analyses. Some elementary adsorption experiments at a fixed conditions were performed to investigate the effects of CeO_2 and Fe_3O_4 contents in chitosan adsorbents on Cr(VI) and Co(II) adsorption. To optimize the adsorption conditions, the response surface methodology (RSM) was used. The effect of solution pH, adsorbent dose, temperature and initial Cr(VI) and Co(II) concentration on the performance of adsorption process was evaluated using central composite design (CCD) of RSM. Furthermore, adsorption kinetics, isotherm and thermodynamics modeling were carried out to analyze the sorption process.

2. Experimental section

2.1. Materials

Cerium nitrate hexahydrate ($Ce(NO_3)_3{\cdot}6H_2O$) (≥99.0%) was purchased from Fluka (Germany) with high purity. Chitosan (95%, molecular weight 200 kDa), oxalic acid (≥99.5%), urea (≥99.5%), acetic acid (≥99.8%), ferric chloride hexahydrate ($FeCl_3{\cdot}6H_2O$) (≥99.0%) and ferrous sulfate heptahydrate ($FeSO_4.7H_2O$) (≥99.5%) were prepared by Merck (Germany). The solvent used for chitosan was glacial acetic acid (Sigma-Aldrich, ≥99.0%). To prepare stock solutions of Cr(VI) and Co(II) ions, the specified amounts of potassium dichromate (Merck, ≥99.9%) and cobalt nitrate hexahydrate (Merck, ≥99.0%) were used. All materials were used as received. Also, deionized water was utilized in the synthesis process of nano-composite and adsorption experiments.

2.2. Synthesis of CeO_2 nanoparticles

First, 14.33 g of $Ce(NO_3)_3{\cdot}6H_2O$, 5.94 g of oxalic acid and 5.96 g of urea were dissolved in a distinct amount of deionized water to prepare the solutions of 0.165 M of $Ce(NO_3)_3{\cdot}6H_2O$, 0.330 M of oxalic acid and 0.495 M of urea, respectively. Thus, a mixture of 1 M solution was obtained. The pH of solution was adjusted to 5.0 by using 36% acetic acid. Then, the volume of solution reached to 200 ml with deionized water under stirring for 120 min. The resulting precipitate was separated by a centrifuge at 3,000 rpm for 20 min and washed with ethanol and deionized water for several times to remove the excess materials from precipitate. Finally, the resulting precursor was calcined at 400°C for 3 h to prepare CeO_2 nanoparticles. It should be mentioned that oxalic acid and urea contributes to the formation of CeO_2 particles on nano-scale without particle aggregation [39].

2.3. Synthesis of Fe_3O_4 nanoparticles

First, 30 mL of 0.75 M $FeCl_3{\cdot}6H_2O$ and 15 mL of 0.75 M $FeSO_4.7H_2O$ were mixed into a 250 mL beaker under stirring. Then, 10 mL of 30% NaOH was dropped into the resulting solution under stirring to form a black precipitate. The resulting magnetic nanoparticles were uniformly dispersed in the solution under stirring for 60 min [40]. After that, the final solution was centrifuged at 3,000 rpm and the precipitate separated by centrifuge was washed with deionized water several times and finally, dried in an oven at 70°C for 12 h.

2.4. Preparation of chitosan/CeO_2/Fe_3O_4 nano-composite adsorbents

For preparation of chitosan solution, 2.5 g of chitosan was added to 200 mL of acetic acid (1%) and stirred for 4 h. This stirring process is carried out to prepare of a homogeneous solution. The pH of solution was adjusted to 5. Then, the

various contents of cerium oxide nanoparticles (0.0–1.2 g) were dispersed in chitosan solution and then mechanically stirred for 3 h to disperse nanoparticles in the solution well. Finally, for synthesis of chitosan/CeO_2 nano-composites, the resulting solution was filtrated and washed with ethanol and deionized water and dried at 60°C for 48 h. For preparation of chitosan/CeO_2/Fe_3O_4 nano-composite, first, different amounts of iron oxide (0.4–1.4 g) were dispersed in chitosan/CeO_2 solution under stirring for 3 h. The operations of filtration, washing and drying were similar to those of mentioned above.

2.5. Characterization of synthesized chitosan/CeO_2/Fe_3O_4 nano-composite adsorbents

To compare the morphology of synthesized samples, FESEM technique was used (SIGMA VP-500 model, Zeiss, Germany). The phase identification of the samples was performed by XRD analysis (X' Pert Pro model, Panalytical, Netherlands) with a Cu K_α radiation in the 2θ range of 10°–80°. The chemical bonds and functional groups of adsorbents were identified by FTIR analysis (RXI model, PerkinElmer, Germany). Also, TEM analysis (Zeiss-EM10C-100 KV model, Germany) was used to investigate the shape of nanoparticles. The surface area, average pore volume and average pore diameter of the samples were determined by BET method (BELSORP model, Japan). Furthermore, the electrical charge of chitosan/CeO_2/Fe_3O_4 nano-composite surface was determined by the point of zero charge pH (pH_{pzc}) as follows. First, 50 mL of 0.1 M NaCl solution was transferred to a series of flasks. Then, the initial pH of each solution was adjusted in the range of 1–7 using 0.1 M NaOH and/or 0.1 M HCl solutions. In the next step, 0.1 g of nano-composite was put in each flask. These flasks were shaken at room temperature for 48 h. After that, the final pH of each solution was specified using a portable pH meter. Finally, pH_{final} values were plotted vs. corresponding $pH_{initial}$ values. The value of pH_{pzc} is a point where the initial pH equals the final pH [41].

2.6. Batch sorption investigations

The adsorption behavior of Cr(VI) and Co(II) ions from aqueous solutions onto the adsorbents was investigated in the flasks containing 25 mL solutions by shaking the flasks at 150 rpm. The effect of CeO_2 and Fe_3O_4 contents was studied on Cr(VI) and Co(II) adsorption at a temperature of 25°C, initial concentration of 200 mg/L, contact time of 100 min with an adsorbent dose of 12.5 mg and pH 5 (adjusted by 0.1 M HCl solution using a pH meter (Switzerland, 827-pH lab, metrohm, Switzerland). The effect of initial concentration, temperature, solution pH and adsorbent dosage on optimization of Cr(VI) and Co(II) adsorption were investigated by RSM. It should be mentioned that the concentration of Cr(VI) and Co(II) ions in the liquid phase was measured using an inductivity coupled plasma spectrophotometer (Aanalys200, PerkinElmer). The adsorption capacity of chitosan/CeO_2/Fe_3O_4 nano-composite adsorbent for Cr(VI) and Co(II) ions was evaluated from the following equation:

$$q_e = \frac{(C_0 - C_e)V}{m} \tag{1}$$

where q_e is the equilibrium adsorption capacity of chitosan/CeO_2/Fe_3O_4 nano-composite for both metal ions (mg/g), C_0 and C_e are the initial and equilibrium Cr(VI) and Co(II) ion concentrations (mg/L), respectively; V is the volume (L) of metal ion solution and m is the amount of dry adsorbent used in adsorption process (g).

2.7. Experimental design for the adsorption of Cr(VI) and Co(II) ions

RSM is used to analyze the adsorption experiments and estimate the relative significance of effective factors and show the interactions between parameters. Also, to optimize the operational conditions to achieve the best adsorption system performance, RSM is applied [42]. Furthermore, the CCD coupled with RSM was employed as an effective approach to evaluate the process conditions and estimate a quadratic model for the response variable [42]. In this research, four independent factors including initial concentration (20–200 mg/L), temperature (20°C–40°C), solution pH (3–9) and adsorbent dosage (10–50 mg) were used for optimization of Cr(VI) and Co(II) ion adsorption. An optimal number of experiments (N) in CCD method can be calculated as follows [43]:

$$N = 2^k + 2k + c_p \tag{2}$$

where k is the number of independent variables; c_p is the number of center points applied to estimate the standard deviation; 2^k is the factorial points and $2k$ is the axial points [43]. It should be mentioned that the higher center points lead to a reduction in pure error. So, CCD with four independent factors involved 2^4 (16) full factorial tests, 8 axial points and 7 replicates at the center points. The input variables including $x_1, x_2, \ldots, x_n$ should be scaled to coded levels. In this study, all four factors in CCD investigated at five coded levels including –1, –0.5, 0, +0.5 and +1. The coded values relates to the real ones by the following equation [44]:

$$x_i = \frac{X_i - X_0}{\Delta X} \tag{3}$$

where x_i represents the dimensionless coded value of the ith independent variable; X_i is the real value; X_0 is the real value at the center point and ΔX shows the value of step change. The quadratic polynomial model was used to fit the experimental data. It is as follows [45,46]:

$$Y = \beta_0 + \sum_{i=1}^{z} \beta_i X_i + \sum_{i=1}^{z-1} \sum_{j=1}^{z} \beta_{ij} X_i X_j + \sum_{i=1}^{z} \beta_{ii} X_i^2 \tag{4}$$

where Y refers to the predicted response; β_0, β_i, β_{ii} and β_{ij} indicate the regression coefficients (the intercept parameter, the linear, the second-order and the interaction effects, respectively); z is the number of factors; X_i represents the coded levels of the independent factors; $X_i X_j$ shows the effect of interactions between parameters and X_i^2 represents the square effect. In order to consider the adequacy of applied regression models, analysis of variance (ANOVA) was used

for adsorption process. The statistical significance of models was checked by *F* value and *p*-value at 95% confidence level. Minitab software was used to analyze the data.

3. Results and discussion

3.1. Characterization of synthesized samples

FESEM images of Fe_3O_4, CeO_2 nanoparticles and chitosan/CeO_2/Fe_3O_4 nano-composite are illustrated in Fig. 1. Fig. 1(a) shows that the most of Fe_3O_4 nanoparticles were uniformly distributed with spherical morphology. The particle size distribution for Fe_3O_4 nanoparticles was in the range of 25–38 nm. Fig. 1(b) shows the irregular CeO_2 crystals. But, most of them had spherical shape. However, the CeO_2 nanoparticles have been well synthesized and their sizes were in the range of 33–69 nm. Fig. 1(c) shows that the Fe_3O_4 and CeO_2 nanoparticles have been uniformly distributed on the chitosan surface with a spherical structure without agglomeration of particles. Furthermore, TEM image of chitosan/CeO_2/Fe_3O_4 nano-composite is shown in Fig. 1(d). As observed, the surface of chitosan has been successfully coated with the Fe_3O_4 and CeO_2 nanoparticles. TEM analysis also confirmed the spherical morphology and uniform distribution of nanoparticles on adsorbent surface. It showed that the average particle size of nanoparticles was found to be 35 nm.

XRD patterns of Fe_3O_4, CeO_2 nanoparticles and chitosan/CeO_2/Fe_3O_4 nano-composite are indicated in Fig. 2. Fig. 2(a) shows the XRD spectrum of Fe_3O_4 nanoparticles. It conformed to the JCPDS standard No. 65-3107. As observed, the crystal surfaces of (220), (311), (400), (511) and (440) were attributed to the Fe_3O_4 phase. Similar results were obtained by others [40]. The position of diffraction peaks of (111), (200), (220), (311), (222), (400), (331) and (420) matched well with those of the CeO_2 nanoparticles (JCPDS standard No. 34-0394) (Fig. 2(b)). No excess peaks are detected in the XRD patterns showing the high purity of the Fe_3O_4 and CeO_2 nanoparticles [31]. Fig. 2(c) indicates the XRD spectrum of chitosan/CeO_2/Fe_3O_4 nano-composite. All of the diffraction peaks in this spectrum confirmed the presence of Fe_3O_4 and CeO_2 nanoparticles in the nano-composite structure. The full obedience of

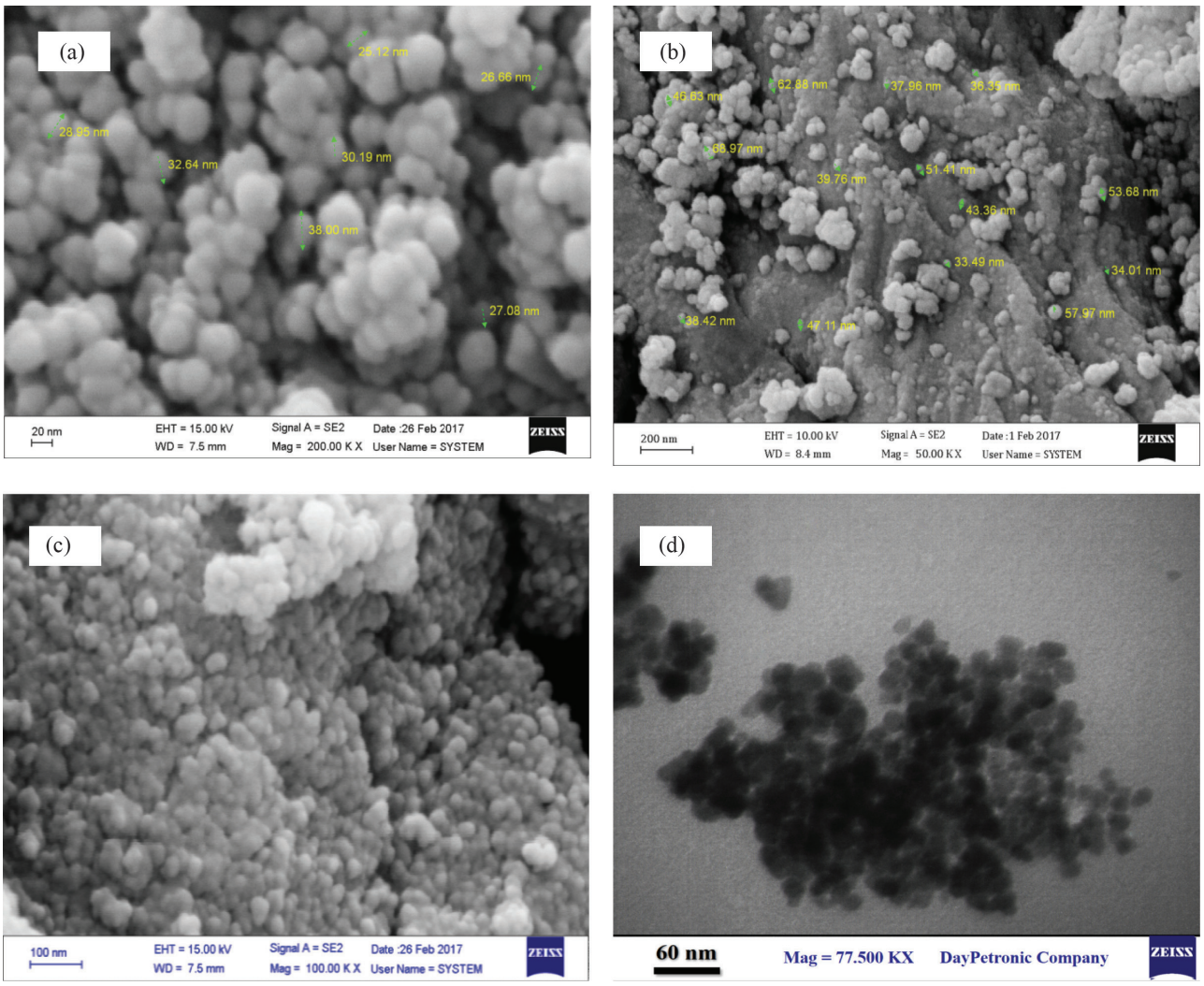

Fig. 1. FESEM images of (a) synthesized Fe_3O_4, (b) CeO_2 nanoparticles, (c) chitosan/CeO_2/Fe_3O_4 and (d) TEM images of chitosan/CeO_2/Fe_3O_4 nano-composite adsorbents.

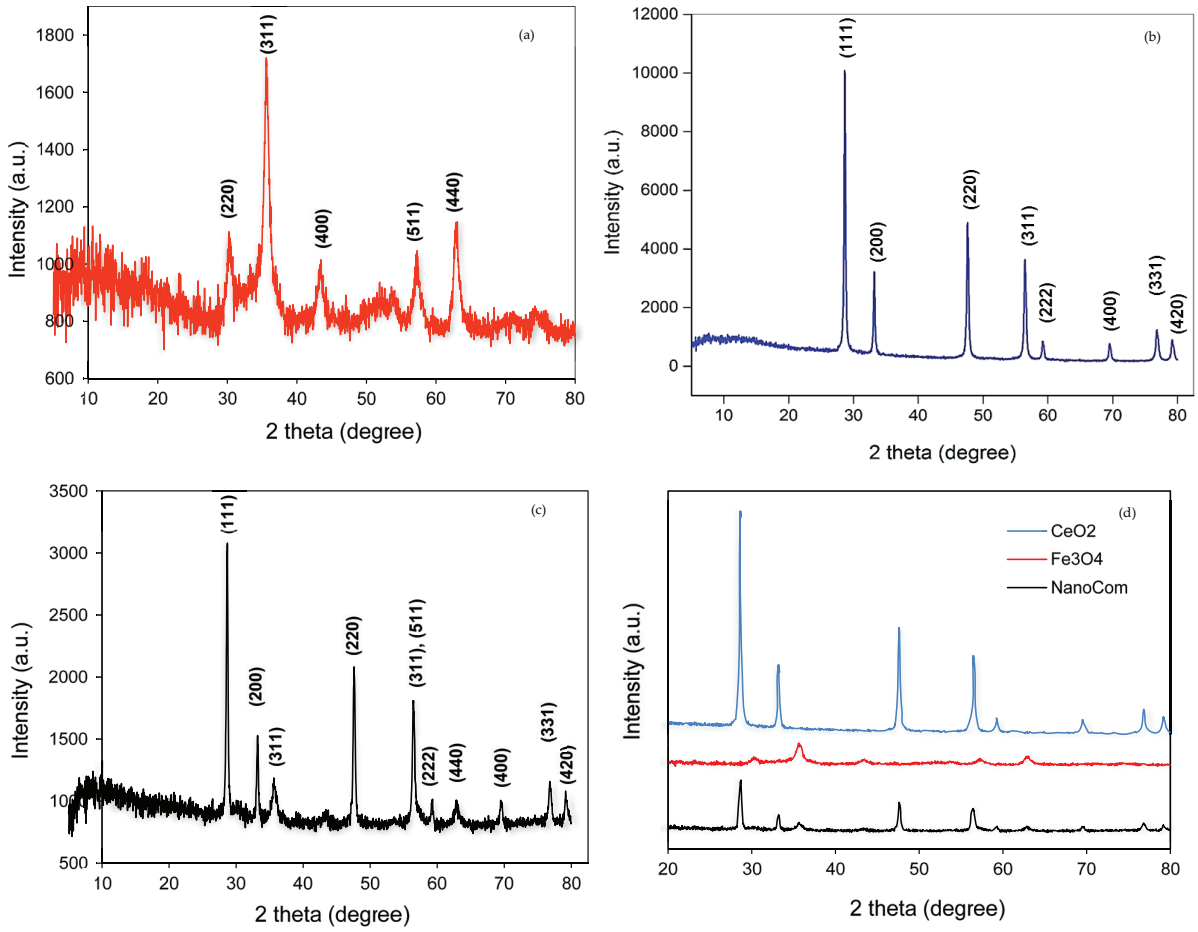

Fig. 2. XRD patterns of synthesized (a) Fe_3O_4, (b) CeO_2 nanoparticles, (c) chitosan/CeO_2/Fe_3O_4 nano-composite and (d) the comparison of XRD patterns.

corresponding peaks of Fe_3O_4 and CeO_2 nanoparticles in XRD pattern of chitosan/CeO_2/Fe_3O_4 nano-composite proved that the nanoparticles structure have been successfully preserved in the nano-composite (Fig. 2(d)).

The FTIR technique was analyzed for the pure chitosan and chitosan/CeO_2/Fe_3O_4 nano-composite adsorbents (before and after adsorption) and the results are shown in Fig. 3. As shown, the absorption peak at 3,430 cm^{-1} was attributed to the stretching vibrations of O–H and N–H groups and the band at 1,550–1,640 cm^{-1} was assigned to the stretching vibrations of amide (N–H) groups. The absorption peak at 2,925 cm^{-1} and 1,050–1,150 cm^{-1} related to C–H and C–O stretching vibrations, respectively. As observed, the broad absorption band at 570–900 cm^{-1} was due to the stretching vibrations of Fe–O and Ce–O in the nano-composite FTIR spectrum confirming the presence of Fe_3O_4 and CeO_2 nanoparticles in the nano-composite structure [35,40]. The FTIR spectra after adsorption of Cr(VI) and Co(II) ions indicated that the corresponding peaks of N–H and –OH groups (3,430), C–H stretching vibrations (2,925 cm^{-1}), N–H groups (1,625 cm^{-1}), Fe–O and Ce–O groups (895 and 610 cm^{-1}) were shifted to the 3,477, 2,930, 1,641, 898 and 620 cm^{-1} after Cr(VI) adsorption and 3,472, 2,927, 1,646, 897 and 618 cm^{-1} after Co(II) adsorption, respectively. As observed in Fig. 3, the peak intensity of –OH, N–H, Fe–O and Ce–O decreased after metal adsorption. This revealed that the chemical interactions between these functional groups of chitosan/CeO_2/Fe_3O_4 nano-composite adsorbent and metal ions (Cr(VI) and Co(II)) were mainly included in the adsorption process.

Based on BET multipoint method, The results are given in Table 1. The results indicated that the S_{BET} and average total pore volume of chitosan/CeO_2 increased remarkably with the increase of CeO_2 contents from 0.25 to 1.0 g. This increase can be due to the presence of CeO_2 nanoparticles in the nano-composite structure. Further increase in CeO_2 contents (1.25 and 1.5 g) led to a decrease in the specific surface area of chitosan/CeO_2 nanocomposite. The S_{BET} and average total pore volume of Chitosan/CeO_2/Fe_3O_4 nano-composites increased with the increase of Fe_3O_4 contents up to 1.2 g. Further increase in Fe_3O_4 contents (1.4 g) resulted in a decrease in total surface area. The reduction of the S_{BET} and average total pore volume of nano-composites with high contents of CeO_2 (1.5 g) and Fe_3O_4 (1.4 g) can be due to the instability of nanoparticles leading to blockage of the pores of adsorbent by agglomeration of nanoparticles. Among the nano-composites, the highest surface area and average pore volume were found to be 118.7 (m^2/g) and 0.0603 (cm^3/g), respectively, for Chitosan/CeO_2/Fe_3O_4 with 1.0 g of CeO_2 and 1.2 g of Fe_3O_4 nanoparticles (Fig. 4).

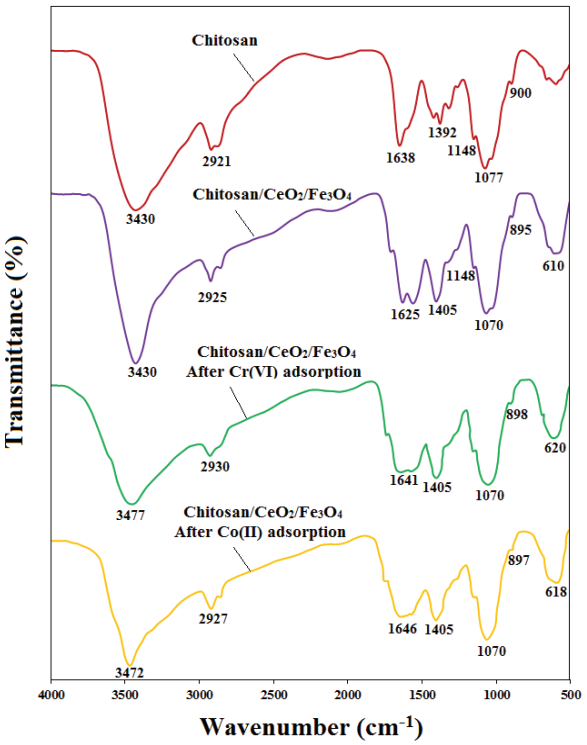

Fig. 3. FTIR analysis for the pure chitosan and chitosan/CeO_2/Fe_3O_4 nano-composite adsorbents (before and after Cr(VI) and Co(II) adsorption).

Table 1
BET surface areas, total pore volumes and average diameters of synthesized nano-composites based on chitosan

Sample	S_{BET} (m^2/g)	V_{toatal} (cm^3/g)	Average diameter (nm)
Chitosan/CeO_2 (0.25 g)	81.2	0.0447	2.451
Chitosan/CeO_2 (1.00 g)	100.5	0.0559	2.312
Chitosan/CeO_2 (1.50 g)	92.8	0.0503	2.396
Chitosan/CeO_2/Fe_3O_4 (0.4 g)	105.0	0.0582	2.302
Chitosan/CeO_2/Fe_3O_4 (1.2 g)	118.7	0.0657	2.214
Chitosan/CeO_2/Fe_3O_4 (1.4 g)	108.5	0.0603	2.283

3.2. Effect of Fe_3O_4 and CeO_2 contents on nano-composite for Cr(VI) and Co(II) adsorption

To investigate the effect of CeO_2 and Fe_3O_4 nanoparticles on the structure of nano-composite, all adsorption experiments were performed at 25°C, initial concentration of 200 mg/L and pH 5 (adjusted by 0.1 M HCl solution) for 100 min with an adsorbent dosage of 0.5 g/L. The effect of CeO_2 contents for adsorption of Cr(VI) and Co(II) ions

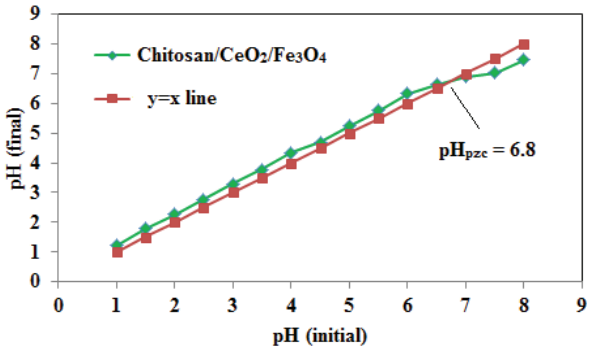

Fig. 4. Determination of point of zero charge (pH_{pzc}) of chitosan/CeO_2/Fe_3O_4 nano-composite adsorbent.

is shown in Figs. 5(a) and (b). As observed, the adsorption capacity of pure chitosan (CeO_2 = 0 wt%) was significantly lower than the adsorption capacity of chitosan/CeO_2 nano-composites for both metal ions (30.1 mg/g for Cr(VI) and 24.3 mg/g for Co(II) ions). After modification of chitosan with CeO_2 nanoparticles, the adsorption capacity increased significantly with the increase of CeO_2 contents from 0.25 to 1.0 g. The adsorption capacity of chitosan/CeO_2 with 0.25 and 1.0 g CeO_2 contents were found to be 52.7 and 114.3 mg/g for Cr(VI) adsorption and 46.7 and 96.5 mg/g for Co(II) adsorption. This enhancement can be due to the increase of surface area with the increase of CeO_2 contents up to 1.0 g. Further increase in CeO_2 contents (1.25 and 1.5 g) resulted in a decrease in adsorption capacity for Cr(VI) and Co(II) ions. This can be due to the unstable CeO_2 nanoparticles with contents of 1.25 and 1.5 g leading to a blockage of adsorbent pores by agglomeration of nanoparticles and a decrease in the adsorption active sites of Cr(VI) and Co(II) ions. Therefore, the optimum amount of CeO_2 content was found to be 1 g. The effect of Fe_3O_4 contents for adsorption of Cr(VI) and Co(II) ions onto the chitosan/CeO_2/Fe_3O_4 nano-composite is shown in Figs. 5(c) and (d). As shown, the adsorption capacity increased significantly with the increase of Fe_3O_4 contents nanoparticles from 0.4 to 1.2 g. It may be due to the increase of surface area with the increase of Fe_3O_4 contents up to 1.2 g. Also, the presence of oxygen in structure of Fe_3O_4 led to the increase of interaction between oxygen electron and metal ions [37]. Further increase in Fe_3O_4 contents (1.4 g) caused to a decrease in adsorption capacity for Cr(VI) and Co(II) ions due to the instability and agglomeration of Fe_3O_4 with high contents. Consequently, the optimum CeO_2 and Fe_3O_4 contents were found to be 1 and 1.2 g in the structure of chitosan/CeO_2/Fe_3O_4 nano-composite adsorbent. Therefore, it was selected for the next adsorption experiments.

3.3. Experimental design and optimization of Cr(VI) and Co(II) adsorption conditions by RSM

The simultaneous effects of four independent variables including initial concentration (X_1), temperature (X_2), solution pH (X_3) and adsorbent dosage (X_4) were studied using RSM according to CCD. The results of predicted and real adsorption capacity for Cr(VI) and Co(II) ions are given in

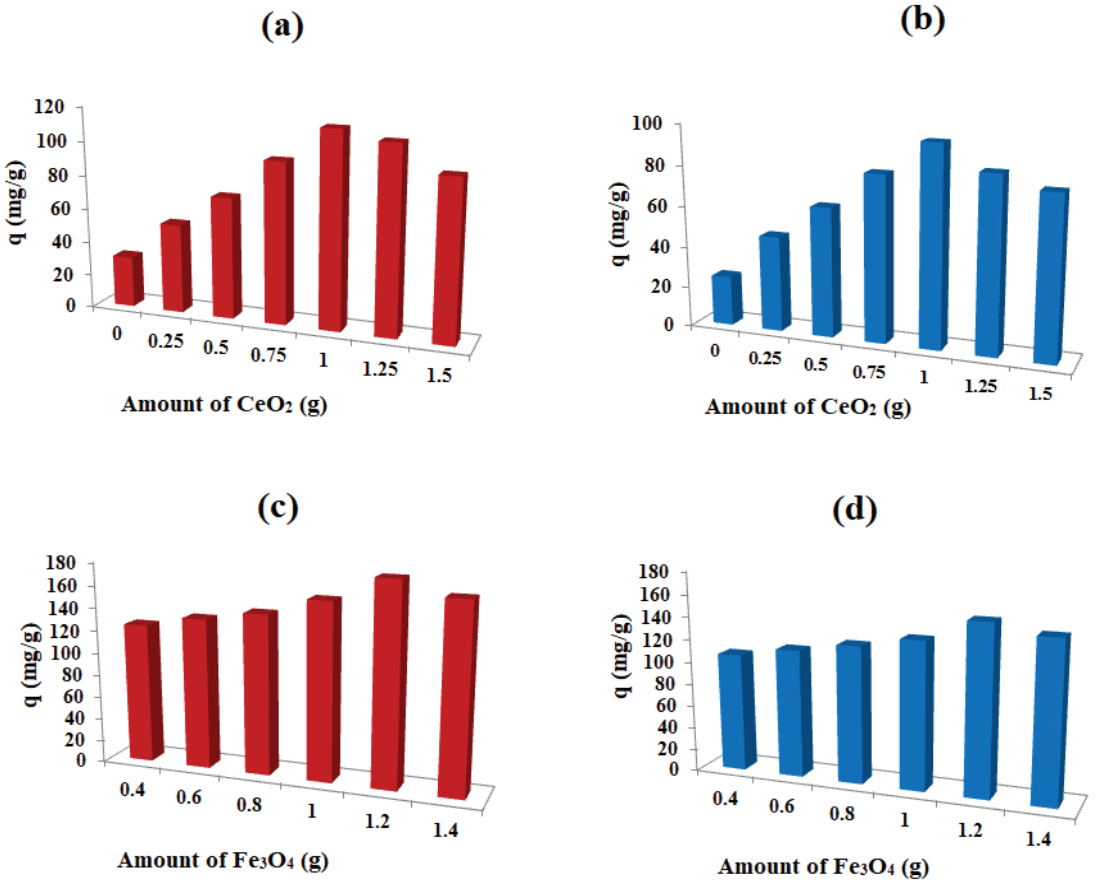

Fig. 5. Effect of CeO_2 contents in the structure of chitosan for (a) Cr(VI) and (b) Co(II) sorption and effect of Fe_3O_4 contents for in the structure of chitosan/CeO_2 adsorbent (c) Cr(VI) and (d) Co(II) sorption (experimental conditions: at temperature of 25°C, initial concentration of 200 mg/L, pH 5, contact time of 100 min with an adsorbent dosage 12.5 mg).

Table 2. The terms in second-order models were determined after excluding insignificant parameters (p-value > 0.1) and the results are given in Table 3. According to p-value and F-value, the final models in terms of coded factors are given as follows (Y_1 is the adsorption capacity for Cr(VI) ions and Y_2 is the adsorption capacity for Co(II) ions):

$$Y_1 = 65.079 + 47.795X_1 - 7.924X_2 - 5.657X_3 - 28.941X_4 - 26.301X_3^2 + 26.407X^2{}_4 - 5.438X_1X_2 - 2.656X_1X_3 - 19.656X_1X_4 + 6.281X_2X_4 \quad (5)$$

$$Y_2 = 44.15 + 40.07X_1 - 2.75X_2 + 7.49X_3 - 34.04X_4 + 13.47X_4^2 + 3.02X_1X_3 - 24.48X_1X_4 + 1.61X_2X_4 - 1.89X_3X_4 \quad (6)$$

The constant values of 65.08 and 44.15 were the offset terms and X_1, X_2, X_3 and X_4 indicated the initial concentration, temperature, solution pH and adsorbent dosage, respectively. The results depicted that the initial concentration with the highest coefficient (47.8 for Cr(VI) and 40.1 for Co(II) ion) had the most important influence on the adsorption capacity. After initial concentration, the adsorbent dosage was an important parameter. On the other hand, only initial concentration had a positive effect on Cr(VI) adsorption and a negative sign for temperature, solution pH and adsorbent dosage showed that adsorption capacity for Cr(VI) ions decreased with the increase of X_2, X_3 and X_4 parameters. While both X_1 and X_3 had a positive effect on Co(II) adsorption. This meant that the adsorption capacity for Co(II) ions increased with increasing the initial concentration and solution pH. Furthermore, both temperature and adsorbent dosage had a negative effect on Co(II) adsorption. Based on ANOVA analysis, the p-values predicted for variables X_1, X_2, X_3, X_4, X_3^2 and X_4^2 for Cr(VI) ions and X_1, X_2, X_3, X_4 and X_4^2 for Co(II) ions were less than 0.05 showing the importance of these variables in adsorption process. Also, p-values of X_1X_2, X_1X_4 and X_2X_4 for Cr(VI) ions and X_1X_3, X_1X_4 and X_3X_4 for Co(II) ions were less than 0.05 showing that they were significant terms in second-order model. The F values of the applied model were found to be 203.3 for Cr(VI) adsorption and 649.5 for Co(II) adsorption corresponding to the p-value less than 0.0001 indicating the adequate of models.

The fit of polynomial equations (Eqs. (5) and (6)) were evaluated by the correlation coefficient (R^2). In this study, R^2 values were found to be 0.9901 and 0.9964 for adsorption capacity for Cr(VI) and Co(II) ions, respectively. This indicated that only 0.99% and 0.36% of the total variables

Table 2
Predicted and actual responses for sorption of Cr(VI) and Co(II) ions onto the chitosan/CeO_2/Fe_3O_4 nano-composite adsorbent (experimental conditions: at a temperature of 20°C, initial concentration of 200 mg/L with adsorbent dosage of 10 mg and with an optimum pH 5.54 for Cr(VI) and pH 9.00 for Co(II) ions)

Experiments	*X*1	*X*2	*X*3	*X*4	Adsorbing capacity(mg/g)			
					Cr(VI)		Co(II)	
					Actual	Predicted	Actual	Predicted
1	1	–1	–1	–1	62.917	65.07851	43.750	44.15426
2	0	0	0	0	62.083	65.07851	43.750	44.15426
3	0	0	0	0	54.583	55.67497	49.583	47.89769
4	0	0	0	–0.5	51.563	57.20969	36.563	30.49935
5	0	0	0	0	66.250	61.33154	37.917	40.41082
6	1	–1	1	–1	33.750	38.44269	22.500	25.16375
7	1	–1	–1	1	27.500	32.44205	37.500	37.88748
8	0.5	0	0	0	9.500	7.31011	5.500	6.603141
9	–1	1	1	–1	7.750	1.309478	9.450	11.75188
10	–1	1	–1	1	67.917	69.04063	47.917	45.52774
11	0	0	0.5	0	95.625	86.15098	59.375	64.54216
12	0	0	-0.5	0	9.000	14.89912	5.000	4.334202
13	0	–0.5	0	0	27.500	20.9067	18.500	16.44481
14	–0.5	0	0	0	7.000	8.898494	9.250	9.482939
15	–1	–1	1	–1	15.000	14.90607	30.000	29.16855
16	1	–1	1	1	73.500	79.77602	32.000	31.63445
17	–1	1	1	1	192.500	189.5336	150.000	148.1201
18	0	0.5	0	0	177.500	172.908	175.000	172.9188
19	0	0	0	0.5	62.500	63.15039	50.000	48.85819
20	0	0	0	0	69.000	65.61503	28.500	29.36552
21	0	0	0	0	150.000	150.2476	140.000	139.4011
22	–1	1	–1	–1	55.000	48.9894	46.000	46.58925
23	–1	–1	1	1	125.000	133.622	162.500	164.1999
24	1	1	–1	1	48.542	41.18078	32.708	24.14643
25	–1	–1	–1	1	89.792	88.97624	60.625	64.16208
26	0	0	0	0	60.417	61.11639	41.667	42.78077
27	1	1	–1	–1	63.750	65.07851	42.917	44.15426
28	–1	–1	–1	–1	63.750	65.07851	44.583	44.15426
29	1	1	1	1	63.333	65.07851	42.917	44.15426
30	1	1	1	–1	62.917	65.07851	42.083	44.15426
31	0	0	0	0	63.750	65.07851	42.917	44.15426

were not clarified by the adsorption capacity for Cr(VI) and Co(II) ions, respectively. The actual and the predicted Cr(VI) and Co(II) adsorption capacity is depicted in Fig. 6. The predicted values were determined using the approximating functions and the actual values were experimental adsorption data [42]. As shown in Fig. 6, the points were located around the $y=x$ line which displayed the correlation of the actual and predicted data and confirmed that the applied models are applicable for the response prediction [47].

The 3D surface plots indicate the interactive influences of two independent parameters (Figs. 7 and 8). Figs. 7(a) and 8(a) indicate the effect of temperature and initial concentration on the adsorption capacity for Cr(VI) and Co(II) ions, respectively. As shown, the maximum Cr(VI) and Co(II) adsorption capacity was obtained at 20°C and initial concentration of 200 mg/L. The sorption capacity for both Cr(VI) and Co(II) ions increased with increasing the initial concentrations. This can be due to the increase in driving force to overcome the mass transfer resistance between adsorbent surface and aqueous solution at higher initial concentration [48,49]. Also, the adsorption capacity increased with the reduction of temperature. It was concluded that the adsorption of both Cr(VI) and Co(II) ions was an exothermic process. The effect of temperature and pH parameters on the adsorption capacity for Cr(VI) and Co(II) ions is illustrated in Figs. 7(b) and 8(b), respectively. As shown in Fig. 7(b), the adsorption capacity for Cr(VI) ions increased with the increase of pH from 3 to 5.54 and decreased with further increase in pH. At very low pH, the dominant species of Cr(VI) are H_2CrO_4 and $HCrO_4^-$; while the two negative dominant species are $HCrO_4^-$ and

Table 3
ANOVA analysis of the fitted quadratic equation for the sorption capacity of chitosan/CeO_2/Fe_3O_4nano-composite adsorbent for Cr(VI) and Co(II) ions (experimental conditions: at a temperature of 20°C, initial concentration of 200 mg/L with adsorbent dosage of 10 mg and with an optimum pH 5.54 for Cr(VI) and pH 9.00 for Co(II) ions)

Cr(VI)					Co(II)			
Source	ΔF	Mean sum of squares	*F* value	*p* value	ΔF	Mean sum of squares	*F* value	*p* value
Regression	10	6,065.0	203.33	0.000	9	6,417.5	649.47	0.000
X_1	1	37,692.7	1,263.63	0.000	1	26,420.7	2,673.84	0.000
X_2	1	1,036.1	34.73	0.000	1	124.5	12.60	0.002
X_3	1	527.9	17.70	0.001	1	924.9	93.60	0.000
X_4	1	13,820.4	463.32	0.000	1	19,122.1	1,935.20	0.000
$^2(X_3)$	1	171.5	5.75	0.026				
$^2(X_4)$	1	172.9	5.79	0.026	1	1,331.5	134.75	0.000
X_1X_2	1	473.1	15.86	0.001				
X_1X_3	1	112.9	3.78	0.066	1	145.8	14.76	0.001
X_1X_4	1	6,181.9	207.24	0.000	1	9,589.3	970.46	0.000
X_2X_4	1	631.3	21.16	0.000	1	41.6	4.21	0.053
X_3X_4					1	57.4	5.81	0.025
Residual	20	29.8			21	9.9		
Lack of fit	14	42.4	109.24	0.000	15	13.6	20.52	
Pure error	6	0.4			6	0.7		
Corrected total	30				30			

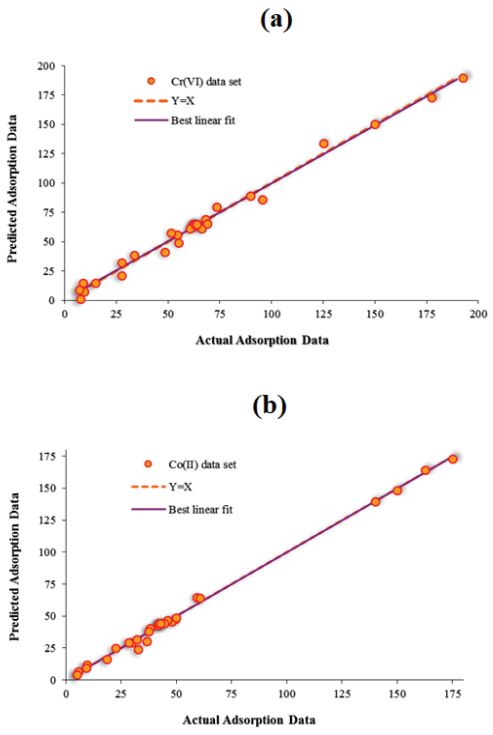

Fig. 6. Predicted vs. actual sorption data for (a) Cr(VI) and (b) Co(II) ions (experimental conditions: at a temperature of 20°C, initial concentration of 200 mg/L with adsorbent dosage of 10 mg and with an optimum pH 5.54 for Cr(VI) and pH 9.00 for Co(II) ions).

$Cr_2O_4^{2-}$ at pH < 6.5; and at pH > 6.5, CrO_4^{2} [50]. On the other hand, the pH_{pzc} of nano-composite adsorbent was 6.8. It is clear that $HCrO_4^-$ and $Cr_2O_4^{2-}$ adsorption onto the active sites requires an adsorbent with positive charge (pH < pH_{pzc}). When pH was very low only $HCrO_4^-$ appeared in the solution and therefore, the adsorption capacity related to the adsorption of only $HCrO_4^-$ species. The optimum pH for Cr(VI) adsorption was found to be 5.54 because the adsorption of both $HCrO_4^-$ and $Cr_2O_4^{2-}$ species occurred. At higher pH (>5.54), the hydroxyl ions increased and the competition of chromium species with hydroxyl ions led to a decrease in adsorption capacity of chitosan/CeO_2/Fe_3O_4 nano-composite. On the other hand, at pH > pH_{pzc}, the nano-composite is negatively charged resulting in an electrostatic repulsion between Cr(VI) anions and active sites of adsorbent [30]. As can be seen in Fig. 8(b), the adsorption capacity for Co(II) ions increased with increasing the pH values because the surface charge of adsorbent became more negative at pH > pH_{pzc} and the main species was Co^{2+} ion. At low pH, the attraction of protons created a protonated surface of adsorbent leading to the competition of Co^{2+} ion and H^+ ions for occupation of the active sites resulted in a lower adsorption for cobalt ions [12]. Therefore, the protonation of functional groups on the adsorbent led to a low adsorption of cationic ions at lower pH [51]. This finding is similar to the literatures reported by Liu et al. [51], and Shi et al. [52]. Figs. 7(c) and 8(c) show the effect of initial concentration and pH on the adsorption capacity. These confirmed the results mentioned above. The highest adsorption capacity was obtained in the initial concentration of 200 mg/L with an optimum pH 5.54 for Cr(VI) ions and 9.00 for Co(II) ions. The effect of adsorbent dosage and initial

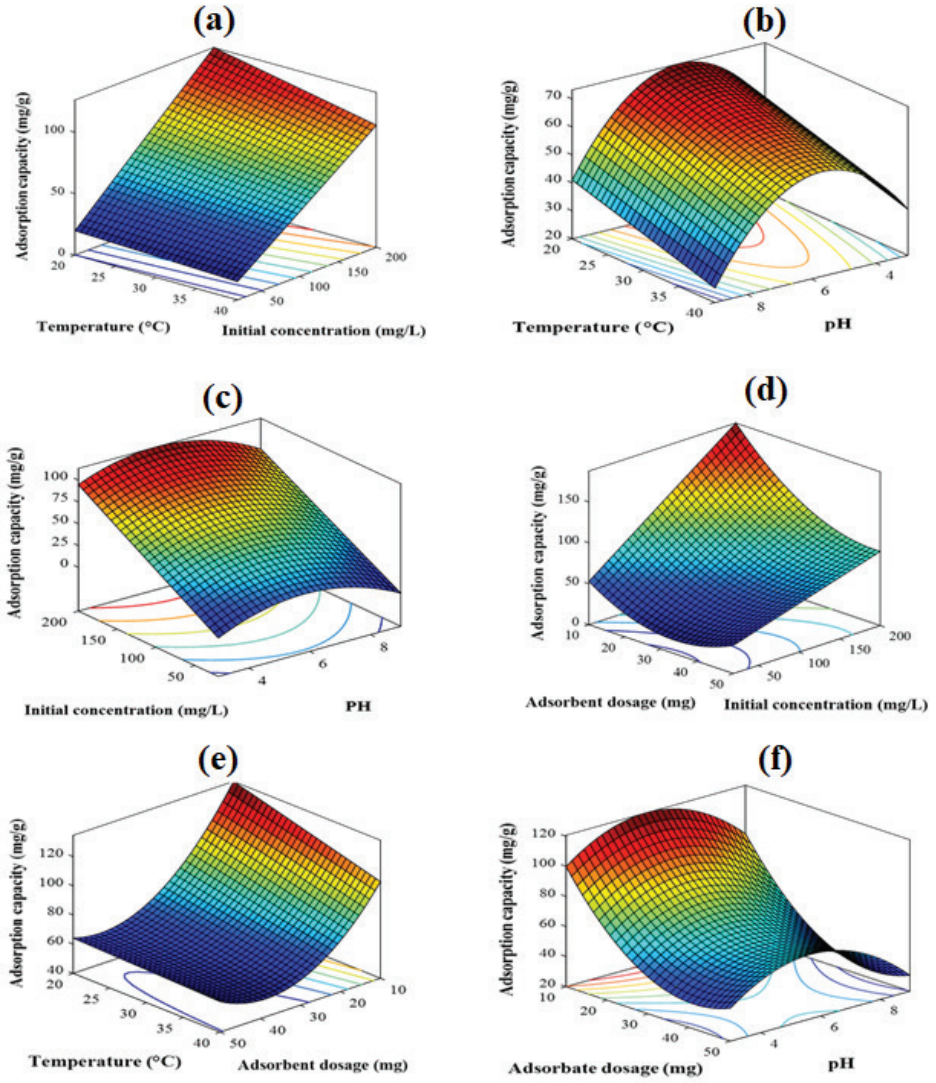

Fig. 7. Three-dimensional response surface graphs of Cr(VI) sorption onto the chitosan/CeO_2/Fe_3O_4 nano-composite adsorbent: the combined effect of (a) temperature and initial concentration, (b) pH and temperature, (c) pH and initial concentration, (d) initial concentration and adsorbent dosage, (e) temperature and adsorbent dosage, (f) adsorbent dosage and pH (experimental conditions: at a temperature of 20°C, initial concentration of 200 mg/L with adsorbent dosage of 10 mg and with an optimum pH 5.54).

concentration, adsorbent dosage and temperature and adsorbent dosage and pH are indicated in Figs. 7(d)–(f) for Cr(VI) ions and Figs. 8(d)–(f) for Co(II) ions, respectively. As shown, the adsorption capacity decreased with the increase of adsorbent dosage from 10 to 50 mg because some of the adsorbent active sites persisted unsaturated through the adsorption process while the number of available sites of the synthesized adsorbent increased with increasing the adsorbent dosage [41]. The results proposed by CCD method depicted that the optimum adsorption conditions for metal ions were determined as initial concentration of 200 mg/L, temperature of 20°C, adsorbent dosage of 10 mg, initial pH 5.54 for Cr(VI) and pH 9.00 for Co(II) ions. The predicted adsorption capacity of chitosan/CeO_2/Fe_3O_4 nano-composite adsorbent for Cr(VI) and Co(II) ions was found to be 208.18 and 172.92 mg/g, respectively, under their optimum conditions.

To verify the results of the model, the confirmation experiments were performed under optimum conditions. The experimental values of adsorption capacity under optimum adsorption conditions for Cr(VI) and Co(II) were found to be 214.21 and 180.1 mg/g, respectively, that was in accordance with their predicted values of adsorption capacity within 2.8% and 3.9% of error for Cr(VI) and Co(II) ions, respectively. These estimated and acceptable errors confirmed the validity of the models.

3.4. Kinetic Cr(VI) and Co(II) adsorption

The effect of contact time on the metal ion adsorption was considered by varying the time from 0 to 100 min, with an initial concentration of 200 mg/L, at a temperature of 20°C with adsorbent dosage of 10 mg and with an optimum pH 5.54 for Cr(VI) and pH 9.00 for Co(II) ions. The results

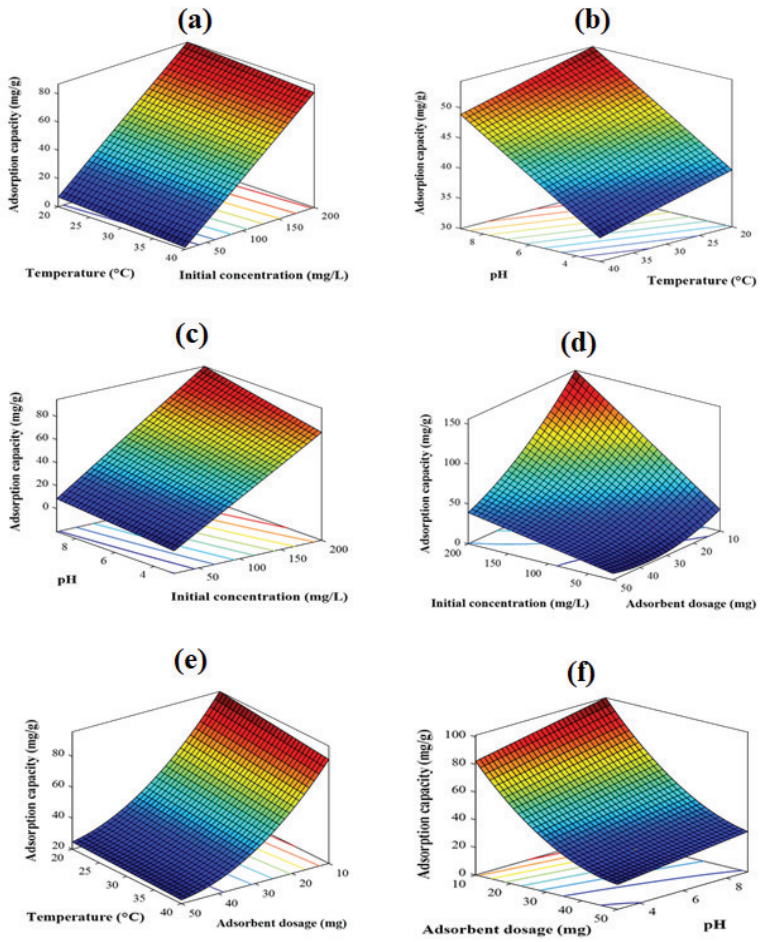

Fig. 8. Three-dimensional response surface graphs of Co(II) sorption onto the chitosan/CeO_2/Fe_3O_4 nano-composite adsorbent: (a) the combined effect of temperature and initial concentration, (b) pH and temperature, (c) pH and initial concentration, (d) initial concentration and adsorbent dosage, (e) temperature and adsorbent dosage, (f) adsorbent dosage and pH (experimental conditions: at a temperature of 20°C, initial concentration of 200 mg/L with adsorbent dosage of 10 mg and with an optimum pH 9.00).

are shown in Fig. 9. As observed, the adsorption process consisted of two steps. The first step is fast within the first 45 min, due to the presence of abundant adsorption sites on adsorbent surface at the beginning of process [51]. The second step is a slower adsorption stage where internal surface diffusion of Cr(VI) and Co(II) ions occurred and the active sites had a tendency to saturate with the increase of contact time up to 100 min. This can be due to the insufficient binding sites of adsorbent at equilibrium time [51]. The similar trends were obtained by others [51,52]. In this work, three kinetic models including the non-linear pseudo-first-order (first reaction-based model), pseudo-second-order (second reaction-based model) and Elovich models were used to simulate the kinetic adsorption of Cr(VI) and Co(II) ions using the MATLAB software. These non-linear models are defined as follows [53–55]:

Pseudo-first-order:

$$q_t = q_e\left(1-\exp(-k_1 t)\right) \tag{7}$$

Pseudo-second-order:

$$q_t = \frac{k_2 q_e^{\,2} t}{1 + k_2 q_e t} \tag{8}$$

Elovich model:

$$q_t = \alpha\,\mathrm{Ln}(t) + \beta \tag{9}$$

where q_t and q_e (mg/g) represent the adsorption capacity at time t and equilibrium time, respectively; k_1 (h^{-1}) and k_2 ($g\,mg^{-1}h^{-1}$) parameters represent the pseudo-first-order and pseudo-second-order sorption rate constants, respectively; α and β are the constants whose chemical importance is not obviously expressed. The kinetic parameters are given in Table 4. The R^2 values of models showed that the consistency between the experimental and theoretical adsorption capacity showed that the kinetics of Cr(VI) and Co(II) adsorption onto the chitosan/CeO_2/Fe_3O_4 adsorbent can be better fitted by pseudo-second-order ($R^2 > 0.999$) in comparison

with pseudo-first-order (R^2 > 0.981) and Elovich models (0.886). The similar trends were obtained by others [51,52]. The Elovich model failed to explain the experimental data well due to the lowest R^2 values. This represented that the chemical-controlling process was rate-limiting step. The similar results were obtained by others [53,54].

3.5. Adsorption isotherm studies

To investigate the adsorption isotherms in Cr(VI) and Co(II) sorption systems, the experiments were performed at a temperature of 20°C, contact time of 100 min with adsorbent dosage of 10 mg and with an optimum pH 5.54 for Cr(VI) and pH 9.00 for Co(II) ions. The adsorption isotherms were analyzed by three different models, namely Langmuir, Freundlich and Temkin models to detect the interaction of metal ions with the synthesized adsorbent. The mathematical approach to evaluate the adsorption behavior can be performed by non-linear isotherm models using MATLAB software. The chemisorption and a monolayer deposition on an adsorbent surface with identical sites are assumed by the Langmuir isotherm model [49,52]. The non-linear Langmuir model can be written as [35,54,55]:

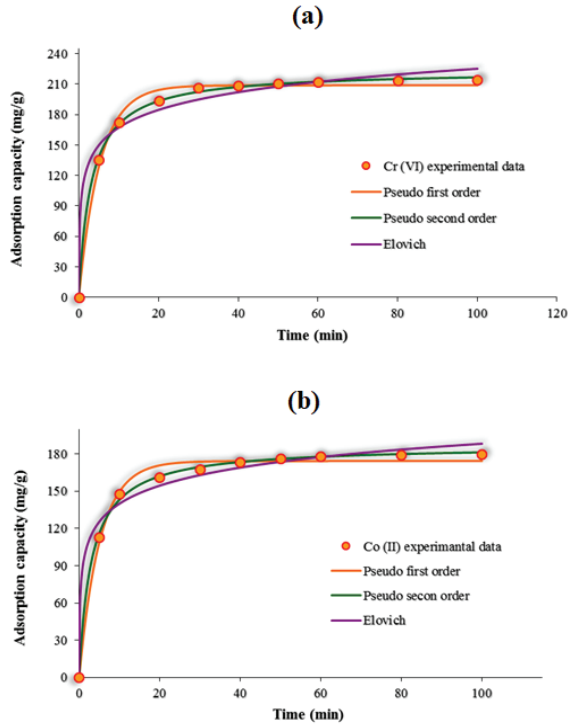

Fig. 9. Effect of contact time on sorption capacity of chitosan/CeO_2/Fe_3O_4 nano-composite adsorbent for (a) Cr(VI) ions and (b) Co(II) ions (experimental conditions: at a temperature of 20°C, initial concentration of 200 mg/L with adsorbent dosage of 10 mg and with an optimum pH 5.54 for Cr(VI) and pH 9.00 for Co(II) ions).

$$q_e = \frac{q_m K_L C_e}{1 + K_L C_e} \tag{10}$$

where q_m (mg/g) is the maximum adsorption capacity, K_L (L/mg) is the rate constant of Langmuir equation corresponding to the energy of adsorption or net enthalpy, C_e (mg/L) is the equilibrium concentration of the heavy metal ions in the solution. The parameter K_L is used to calculate a dimensionless separation factor (R_L) by the following equation [55]:

$$R_L = \frac{1}{1 + K_L C_0} \tag{11}$$

where C_0 represents the highest initial Cr(VI) and Co(II) concentrations. The R_L values show that the adsorption is irreversible (R_L = 0), favorable (0 < R_L<1), linear (R_L = 0) and unfavorable (R_L > 1).

The Freundlich model describes the exponential distribution, multilayer adsorption and heterogonous adsorption energies of active sites on the adsorbent surface. Also, this model represents that the surface saturation does not occur therefore, infinite surface coverage is expected. The non-linear expression of Freundlich model can be written as [56,57]:

$$q_e = K_F C_e^{1/n} \tag{12}$$

where K_F ((mg/g)/(l/mg)$^{1/n}$) and n are both the Freundlich isotherm constants. K_F represents the adsorption capacity and n is the heterogeneity factor relating to the intensity of the adsorption. Values of n should be greater than 1 for the feasible adsorption [20,58].

Temkin isotherm model assumes that the adsorption heat of all molecules in the layer declines with coverage because of the adsorbent–metal ion interactions. The non-linear Temkin model can be written as [59]:

$$q_e = A_T \ln (B_T C_e) \tag{13}$$

where $A_T = RT/b_T$, R (kJ mol^{-1} K^{-1}) and T (K) represent the universal gas constant and absolute temperature, respectively.

Table 4
Parameters of applied kinetic models for Cr(VI) and Co(II) ion sorption onto the chitosan/CeO_2/Fe_3O_4nano-composite adsorbent (experimental conditions: at a temperature of 20°C, initial concentration of 200 mg/L with adsorbent dosage of 10 mg and with an optimum pH 5.54 for Cr(VI) and pH 9.00 for Co(II) ions)

Contaminants	Pseudo-first-order model			Pseudo-second-order model			Elovich model		
	q_e (mg/g)	K_1 (1/h)	R^2	q_e (mg/g)	K_2 (g/(mg h)	R^2	β	α	R^2
Cr(VI)	209.1	0.1901	0.9934	223.5	0.001438	0.9992	0.0396	1,910	0.8862
Co(II)	175.1	0.1509	0.9915	190.5	0.00121	0.9991	0.03814	384.2	0.9141

The constant of b_T (kJ/mol) is ascribed to the heat of adsorption and B_T (L/g) explains the maximum binding energy.

The isotherm model parameters are given in Table 5. The adsorption equilibrium data of both Cr(VI) and Co(II) ions onto the chitosan/CeO_2/Fe_3O_4 nano-composite adsorbent fitted well with the Langmuir isotherm model with the highest R^2 (>0.992) compared with the other models. This suggested that the adsorption of each molecule onto the active sites had the same activation energies [58]. The maximum adsorption capacity (q_m) of chitosan/CeO_2/Fe_3O_4 nano-composite adsorbent was found to be 316.1 and 263.6 mg/g at 20°C for Cr(VI) and Co(II) ions, respectively. For the current adsorption system, R_L values for Cr(VI) and Co(II) ions were 0.227 and 0.255 indicating the favorability of the adsorption process. Also, the favorable sorption of Cr(VI) and Co(II) ions was confirmed by n values obtained from Freundlich model (n > 1) [55,60]. As shown, the B_T (L/g) value of Cr(VI) ions (0.219 L/g) was greater than that of Co(II) ions (0.164 L/g) showing that interactions between adsorbent–metal ions were more effective for Cr(VI) compared with Co(II) ions. The similar results were obtained by others [59].

Furthermore, the maximum adsorption capacity of chitosan/CeO_2/Fe_3O_4 nano-composite was compared with other adsorbents synthesized by others for removal of Cr(VI) and Co(II) ions from water systems (Table 6). The results indicated that q_m (mg/g) of synthesized chitosan/CeO_2/Fe_3O_4 nano-composite in the current work was greater than that of other adsorbents. This may be due to the presence of all –OH, N–H, Fe–O and Ce–O groups in the structure of the synthesized nano-composite compared with other adsorbents (confirmed by FTIR analysis). A decrease in peak intensity of –OH, N–H, Fe–O and Ce–O after metal adsorption revealed the chemical interactions between these functional groups of chitosan/CeO_2/Fe_3O_4 nano-composite adsorbent and metal ions (Cr(VI) and Co(II)) ions. Similar results were obtained by Liu et al. [51], and Shi et al. [52]. Therefore, the invesigation of adsorption mechanism is necessary.

The suggested adsorption mechanism of Cr(VI) and Co(II) ions were also investigated and shown in Fig. 10. Indeed, there are dominant anionic Cr(VI) species such as $HCrO_4^-$ and $Cr_2O_4^{2-}$ in the aqueous solution at pH 5.54. As observed in Fig. 10, the chitosan/CeO_2/Fe_3O_4 nano-composite adsorbent

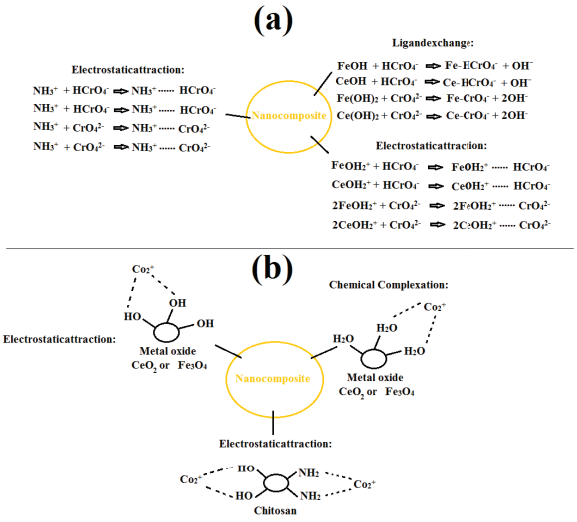

Fig. 10. Suggested adsorption mechanism of Cr(VI) and Co(II) ions from aqueous solution onto the chitosan/CeO_2/Fe_3O_4.

Table 5
Parameters of applied isotherm models for Cr(VI) and Co(II) ion sorption onto the chitosan/CeO_2/Fe_3O_4 nano-composite adsorbent (experimental conditions: at a temperature of 20°C, initial concentration of 200 mg/L with adsorbent dosage of 10 mg and with an optimum pH 5.54 for Cr(VI) and pH 9.00 for Co(II) ions)

Contaminates	Freundlich model			Langmuir model			Temkin model		
	n	K_F $^{1/n}$(l/mg)(mg/g)	R^2	q_m (mg/g)	K_L (l/mg)	R^2	A_T	B_T (l/g)	R^2
Cr(VI)	2.122	21.33	0.9734	316.1	0.01705	0.9945	63.47	0.2193	0.9862
Co(II)	2.106	16.36	0.9433	263.57	0.0146	0.9924	55.47	0.1644	0.9812

Table 6
Comparison of maximum adsorption capacity of chitosan/CeO_2/Fe_3O_4 nano-composite adsorbent with other adsorbents

Adsorbents	q_{max} (mg/g) for Cr(VI) ions	q_{max} (mg/g) for Co(II) ions	Reference
Cross-linked chitosan magnetic beads	138.50	–	[53]
Synthesized CeO_2 nanoparticles	121.90	–	[31]
APTES/TMPTMS/zirconia/PVP/P123	–	179.73	[60]
Magnetic MWCNT/IO composites	–	10.61	[12]
Almond green hull	–	45.50	[14]
Silane-modified halloysite/Fe_3O_4	59.90	–	[64]
Chitosan benzoyl thiourea derivative	–	29.47	[65]
Nano iron oxide impregnated in chitosan	–	88.30	[11]
Magnetite Fe_3O_4 nanoparticles-chitosan	–	39.50	[13]
Chitosan/CeO_2/Fe_3O_4 nano-composite	316.1	263.57	This work

Table 7
Thermodynamic parameters for Cr(VI) and Co(II) ion sorption onto the chitosan/CeO_2/Fe_3O_4 nano-composite adsorbent (experimental conditions: at a temperature of 20°C, initial concentration of 200 mg/L with adsorbent dosage of 10 mg and with an optimum pH 5.54 for Cr(VI) and pH 9.00 for Co(II) ions)

Contaminants	−Δ*G* (kJ/mol)				−Δ*S* (kJ/mol K)	−Δ*H* (kJ/mol)	R^2
	293 (K)	303 (K)	313 (K)	323 (K)			
Cr(VI)	1.523	1.33	1.14	0.943	0.0194	7.21	0.9876
Co(II)	0.864	0.728	0.590	0.452	0.0138	4.91	0.9722

contains functional groups such as Fe–OH_2^+, Ce–OH_2^+ and NH_3^+ for the electrostatic attraction which is one of the adsorption mechanism. Also, other groups such as Ce–OH, Fe–OH and hydroxyl surface play an important role in ligand exchange [11]. The adsorption mechanism of Co(II) ions contains electrostatic attraction and chemical complexation (or electron exchange from the surface of nano-composite to Co(II) ions). The surface hydroxyl groups of chitosan/CeO_2/Fe_3O_4 nano-composite adsorbent may be dissociated into –O– groups and adsorbed the positively charged cobalt ions.

3.6. Thermodynamic investigation

Thermodynamic parameters such as Gibbs energy change (Δ*G*°), enthalpy change (Δ*H*°) and entropy change (Δ*S*°) give supplementary in-depth information about inherent energetic changes corresponding to the adsorption process. The standard Gibbs free energy is shown as follows [55]:

$$\Delta G^{\circ} = -RT\ln K_C \tag{14}$$

where *R* (8.3145 J/(mol K)) is the ideal gas constant, *T* (K) is the absolute temperature and K_c is the thermodynamic equilibrium constant. The relationship between K_c and temperature is given by the Van't Hoff equation [61,62]:

$$\ln(K_c) = \frac{\Delta S^{\circ}}{R} - \frac{\Delta H^{\circ}}{R} \times \frac{1}{T} \tag{15}$$

Thus, Δ*H*° and Δ*S*° parameters can be estimated from slope and intercept of plotted ln(K_c) vs. 1/*T* linear, respectively (figure is not shown). The Cr(VI) and Co(II) adsorption process onto the chitosan/CeO_2/Fe_3O_4 nano-composite was investigated at different temperatures (25°C–45°C) to estimate the thermodynamics parameters. All the thermodynamic data are given in Table 7. The negative values of Δ*G*° for both Cr(VI) and Co(II) ions showed the spontaneity of sorption process. The values of Δ*G*° were in the range of 0 to –20 kJ/mol which indicated a dominant physical sorption and weak chemisorption of Cr(VI) and Co(II) ions onto the nano-composite adsorbent. Similar results were obtained by others [63]. Also, Δ*G*° values decreased with the increase of temperature from 25°C to 45°C leading to a higher adsorption of Cr(VI) and Co(II) ions at lower temperature. The negative values of Δ*H*° suggested that the adsorption process was exothermic. Based on Δ*S*° values, there are associative and dissociative mechanisms. When Δ*S*° > –10 J mol^{-1} K^{-1}, the dissociative mechanism becomes dominant [48]. In this study, Δ*S*° for Cr(VI) and Co(II) were greater than –10 J mol^{-1} K^{-1} indicated that the adsorption process followed the dissociative mechanism. This showed that the ratio of free Cr(VI) and Co(II) ions to ions interacting with the adsorbent will be higher than the adsorbed state [48].

4. Conclusion

An effective chitosan/CeO_2/Fe_3O_4 nano-composite adsorbent was used to evaluate the removal of Cr(VI) and Co(II) ions from aqueous solutions. The characterization of adsorbents was investigated by FESEM, TEM, FTIR, BET and XRD analyses. The spherical morphology and uniform distribution of nanoparticles on adsorbent surface were confirmed by FESEM and TEM. The total S_{BET}, average pore volume and average pore diameter of chitosan/CeO_2/Fe_3O_4 nano-composite adsorbent were found to be 118.7 m^2/g, 0.066 cm^3/g and 2.21 nm, respectively. The RSM was applied to obtain the optimum adsorption conditions for Cr(VI) and Co(II) ions. The optimal adsorption conditions were initial concentration of 200 mg/L, temperature of 20°C, adsorbent dosage of 10 mg, initial pH 5.54 for Cr(VI) and pH 9.00 for Co(II) ions. The predicted models showed that the initial metal ion concentration with the highest coefficient was the most effective parameter on the adsorption capacity for both Cr(VI) and Co(II) ions. The experimental adsorption data perfectly fitted the pseudo-second-order kinetic model and Langmuir isotherm model. The maximum adsorption capacity for Cr(VI) and Co(II) ions obtained from Langmuir model were 316.10 and 263.57 mg/g, respectively. The negative values of Δ*G*° and Δ*H*° for both Cr(VI) and Co(II) ions showed that the nature of adsorption process was spontaneous and exothermic.

References

[1] H.N. Bhatti, A. Jabeen, M. Iqbal, S. Noreen, Z. Naseem, Adsorptive behavior of rice bran-based composites for malachite green dye: isotherm, kinetic and thermodynamic studies, J. Mol. Liq., 237 (2017) 322–333.
[2] S. Ghezali, A. Mahdad-Benzerdjeb, M. Ameri, A.Z. Bouyakoub, Adsorption of 2, 4, 6-trichlorophenol on bentonite modified with benzyldimethyltetradecylammonium chloride, Chem. Int., 4 (2018) 24–32.
[3] A. Kausar, G. MacKinnon, A. Alharthi, J. Hargreaves, H.N. Bhatti, M. Iqbal, A green approach for the removal of Sr (II) from aqueous media: kinetics, isotherms and thermodynamic studies, J. Mol. Liq., 257 (2018) 164–172.
[4] S. Shoukat, H.N. Bhatti, M. Iqbal, S. Noreen, Mango stone biocomposite preparation and application for crystal violet adsorption: a mechanistic study, Microporous Mesoporous Mater., 239 (2017) 180–189.

[5] N. Tahir, H.N. Bhatti, M. Iqbal, S. Noreen, Biopolymers composites with peanut hull waste biomass and application for Crystal Violet adsorption, Int. J. Biol. Macromol., 94 (2017) 210–220.
[6] Y. Bulut, Removal of heavy metals from aqueous solution by sawdust adsorption, J. Environ. Sci., 19 (2007) 160–166.
[7] Y.A. El-Reash, A. Abdelghany, A.A. Elrazak, Removal and separation of Cu (II) from aqueous solutions using nano-silver chitosan/polyacrylamide membranes, Int. J. Biol. Macromol., 86 (2016) 789–798.
[8] A. Gupta, C. Balomajumder, Simultaneous adsorption of Cr (VI) and phenol onto tea waste biomass from binary mixture: multicomponent adsorption, thermodynamic and kinetic study, J. Environ. Chem. Eng., 3 (2015) 785–796.
[9] M. Abbas, M. Adil, S. Ehtisham-ul-Haque, B. Munir, M. Yameen, A. Ghaffar, G.A. Shar, M.A. Tahir, M. Iqbal, *Vibrio fischeri* bioluminescence inhibition assay for ecotoxicity assessment: a review, Sci. Total Environ., 626 (2018) 1295–1309.
[10] M. Iqbal, *Vicia faba* bioassay for environmental toxicity monitoring: a review, Chemosphere, 144 (2016) 785–802.
[11] J. Lu, K. Xu, J. Yang, Y. Hao, F. Cheng, Nano iron oxide impregnated in chitosan bead as a highly efficient sorbent for Cr (VI) removal from water, Carbohydr. Polym., 173 (2017) 28–36.
[12] Q. Wang, J. Li, C. Chen, X. Ren, J. Hu, X. Wang, Removal of cobalt from aqueous solution by magnetic multiwalled carbon nanotube/iron oxide composites, Chem. Eng. J., 174 (2011) 126–133.
[13] T.I. Shalaby, N. Fikrt, M. Mohamed, M. El Kady, Preparation and characterization of iron oxide nanoparticles coated with chitosan for removal of Cd (II) and Cr (VI) from aqueous solution, Water Sci. Technol., 70 (2014) 1004–1010.
[14] A. Ahmadpour, M. Tahmasbi, T.R. Bastami, J.A. Besharati, Rapid removal of cobalt ion from aqueous solutions by almond green hull, J. Hazard. Mater., 166 (2009) 925–930.
[15] S.S. Hamdan, M.H. El-Naas, Characterization of the removal of chromium (VI) from groundwater by electrocoagulation, J. Ind. Eng. Chem., 20 (2014) 2775–2781.
[16] C.J. Sun, M.G. Li, S.H. Gau, Y.H. Wang, Y.L. Jan, Improving the mechanical characteristics and restraining heavy metal evaporation from sintered municipal solid waste incinerator fly ash by wet milling, J. Hazard. Mater., 195 (2011) 281–290.
[17] M. Taseidifar, F. Makavipour, R.M. Pashley, A.M. Rahman, Removal of heavy metal ions from water using ion flotation, Environ. Technol. Innov., 8 (2017) 182–190.
[18] M. Coll, A. Fortuny, C. Kedari, A. Sastre, Studies on the extraction of Co (II) and Ni (II) from aqueous chloride solutions using Primene JMT-Cyanex272 ionic liquid extractant, Hydrometallurgy, 125 (2012) 24–28.
[19] F. Becker, D. Rodríguez, M. Schwab, Magnetic removal of cobalt from waste water by ferrite co-precipitation, Procedia. Mater. Sci., 1 (2012) 644–650.
[20] H. Demey, T. Vincent, E. Guibal, A novel algal-based sorbent for heavy metal removal, Chem. Eng. J., 332 (2018) 582–595.
[21] M. Akram, H.N. Bhatti, M. Iqbal, S. Noreen, S. Sadaf, Biocomposite efficiency for Cr(VI) adsorption: kinetic, equilibrium and thermodynamics studies, J. Environ. Chem. Eng., 5 (2017) 400–411.
[22] P. Author, Kinetic study of Cr(III) and Cr(VI) biosorption using Rosa damascena phytomass: a rose waste biomass, Asian J. Chem., 25 (2013) 2099–2103.
[23] H.N. Bhatti, Q. Zaman, A. Kausar, S. Noreen, M. Iqbal, Efficient remediation of Zr(IV) using citrus peel waste biomass: kinetic, equilibrium and thermodynamic studies, Ecol. Eng., 95 (2016) 216–228.
[24] I.A. Bhatti, N. Ahmad, N. Iqbal, M. Zahid, M. Iqbal, Chromium adsorption using waste tire and conditions optimization by response surface methodology, J. Environ. Chem. Eng., 5 (2017) 2740–2751.
[25] A. Kausar, H.N. Bhatti, M. Iqbal, A. Ashraf, Batch versus column modes for the adsorption of radioactive metal onto rice husk waste: conditions optimization through response surface methodology, Water Sci. Technol., 76 (2017) 1035–1043.
[26] Q. Meng, H. Chen, J. Lin, Z. Lin, J. Sun, Zeolite A synthesized from alkaline assisted pre-activated halloysite for efficient heavy metal removal in polluted river water and industrial wastewater, J. Environ. Sci., 56 (2017) 254–262.
[27] X. Yu, S. Tong, M. Ge, L. Wu, J. Zuo, C. Cao, W. Song, Adsorption of heavy metal ions from aqueous solution by carboxylated cellulose nanocrystals, J. Environ. Sci., 25 (2013) 933–943.
[28] A. Contreras, E. Casals, V. Puntes, D. Komilis, A. Sánchez, X. Font, Use of cerium oxide (CeO_2) nanoparticles for the adsorption of dissolved cadmium (II), lead (II) and chromium (VI) at two different pHs in single and multi-component systems, Global Nest J., 17 (2015) 536–543.
[29] P.N. Dave, L.V. Chopda, Application of iron oxide nanomaterials for the removal of heavy metals, J. Nanotechnol., 2014 (2014) 1–14.
[30] N. Ilankoon, Use of iron oxide magnetic nanosorbents for Cr (VI) removal from aqueous solutions: a review, J. Eng. Res. Appl., 4 (2014) 55–63.
[31] S. Recillas, J. Colón, E. Casals, E. González, V. Puntes, A. Sánchez, X. Font, Chromium VI adsorption on cerium oxide nanoparticles and morphology changes during the process, J. Hazard. Mater., 184 (2010) 425–431.
[32] R. Taman, M. Ossman, M. Mansour, H. Farag, Metal oxide nano-particles as an adsorbent for removal of heavy metals, J. Adv. Chem. Eng., 5 (2015) 125.
[33] N. Pojananukij, K. Wantala, S. Neramittagapong, A. Neramittagapong, Equilibrium, kinetics, and mechanism of lead adsorption using zero-valent iron coated on diatomite, Desal. Wat. Treat., 57 (2016) 18475–18489.
[34] P.Z. Ray, H.J. Shipley, Inorganic nano-adsorbents for the removal of heavy metals and arsenic: a review, RSC Adv., 5 (2015) 29885–29907.
[35] S. Yari, S. Abbasizadeh, S.E. Mousavi, M.S. Moghaddam, A.Z. Moghaddam, Adsorption of Pb (II) and Cu (II) ions from aqueous solution by an electrospun CeO_2 nanofiber adsorbent functionalized with mercapto groups, Process Saf. Environ. Protect., 94 (2015) 159–171.
[36] A. Bhatnagar, M. Sillanpää, Applications of chitin-and chitosan-derivatives for the detoxification of water and wastewater—a short review, Adv. Colloid Interface Sci., 152 (2009) 26–38.
[37] M. Keshvardoostchokami, L. Babaei, A. Zamani, A. Parizanganeh, F. Piri, Synthesized chitosan/iron oxide nanocomposite and shrimp shell in removal of nickel, cadmium and lead from aqueous solution, Global J. Environ. Sci. Manage., 3 (2017) 267–278.
[38] H. Jiang, P. Chen, S. Luo, X. Tu, Q. Cao, M. Shu, Synthesis of novel nanocomposite Fe_3O_4/ZrO_2/chitosan and its application for removal of nitrate and phosphate, Appl. Surf. Sci., 284 (2013) 942–949.
[39] J. Sun, C. Wang, L. Zeng, P. Xu, X. Yang, J. Chen, X. Xing, Q. Jin, R. Yu, Controllable assembly of CeO_2 micro/nanospheres with adjustable size and their application in Cr(VI) adsorption, Mater. Res. Bull., 75 (2016) 110–114.
[40] V. Sureshkumar, S.K. Daniel, K. Ruckmani, M. Sivakumar, Fabrication of chitosan–magnetite nanocomposite strip for chromium removal, Appl. Nanosci., 6 (2016) 277–285.
[41] S. Abbasizadeh, A.R. Keshtkar, M.A. Mousavian, Preparation of a novel electrospun polyvinyl alcohol/titanium oxide nanofiber adsorbent modified with mercapto groups for uranium (VI) and thorium (IV) removal from aqueous solution, Chem. Eng. J., 220 (2013) 161–171.
[42] A. Özer, G. Gürbüz, A. Çalimli, B.K. Körbahti, Biosorption of copper (II) ions on *Enteromorpha prolifera*: application of response surface methodology (RSM), Chem. Eng. J., 146 (2009) 377–387.
[43] A. Özer, G. Gürbüz, A. Çalimli, B.K. Körbahti, Investigation of nickel (II) biosorption on *Enteromorpha prolifera*: optimization using response surface analysis, J. Hazard. Mater., 152 (2008) 778–788.
[44] G.H. Mirzabe, A.R. Keshtkar, Application of response surface methodology for thorium adsorption on PVA/Fe_3O_4/SiO_2/APTES nanohybrid adsorbent, J. Ind. Eng. Chem., 26 (2015) 277–285.

[45] M. Khayet, C. Cojocaru, M. Essalhi, Artificial neural network modeling and response surface methodology of desalination by reverse osmosis, J. Membr. Sci., 368 (2011) 202–214.
[46] A. Najafpoor, H. Alidadi, H. Esmaeili, T. Hadilou, M. Dolatabadi, A. Hosseinzadeh, M. Davoudi, Optimization of anionic dye adsorption onto *Melia azedarach* sawdust in aqueous solutions: effect of calcium cations, Asia-Pac. J. Chem. Eng., 11 (2016) 258–270.
[47] M. Arshadi, S. Mousavi, Simultaneous recovery of Ni and Cu from computer-printed circuit boards using bioleaching: statistical evaluation and optimization, Bioresour. Technol., 174 (2014) 233–242.
[48] S. Abbasizadeh, A.R. Keshtkar, M.A. Mousavian, Sorption of heavy metal ions from aqueous solution by a novel cast PVA/TiO_2 nanohybrid adsorbent functionalized with amine groups, J. Ind. Eng. Chem., 20 (2014) 1656–1664.
[49] M. Bozorgi, S. Abbasizadeh, F. Samani, S.E. Mousavi, Performance of synthesized cast and electrospun PVA/chitosan/ZnO-NH_2 nano-adsorbents in single and simultaneous adsorption of cadmium and nickel ions from wastewater, Environ. Sci. Pollut. Res., 25 (2018) 17457–17472.
[50] C.-C. Kan, A.H. Ibe, K.K.P. Rivera, R.O. Arazo, M.D.G. de Luna, Hexavalent chromium removal from aqueous solution by adsorbents synthesized from groundwater treatment residuals, Sustain. Environ. Res., 27 (2017) 163–171.
[51] T. Liu, X. Han, Y. Wang, L. Yan, B. Du, Q. Wei, D. Wei, Magnetic chitosan/anaerobic granular sludge composite: synthesis, characterization and application in heavy metal ions removal, J. Colloid Interface Sci., 508 (2017) 405–414.
[52] L. Shi, D. Wei, H.H. Ngo, W. Guo, B. Du, Q. Wei, Application of anaerobic granular sludge for competitive biosorption of methylene blue and Pb(II): fluorescence and response surface methodology, Bioresour. Technol., 194 (2015) 297–304.
[53] Y.A. El-Reash, Magnetic chitosan modified with cysteine-glutaraldehyde as adsorbent for removal of heavy metals from water, J. Environ. Chem. Eng., 4 (2016) 3835–3847.
[54] G. Sheng, D. Shao, X. Ren, X. Wang, J. Li, Y. Chen, X. Wang, Kinetics and thermodynamics of adsorption of ionizable aromatic compounds from aqueous solutions by as-prepared and oxidized multiwalled carbon nanotubes, J. Hazard. Mater., 178 (2010) 505–516.
[55] M. Talebi, S. Abbasizadeh, A.R. Keshtkar, Evaluation of single and simultaneous thorium and uranium sorption from water systems by an electrospun PVA/SA/PEO/HZSM5 nanofiber, Process Saf. Environ. Protect., 109 (2017) 340–356.
[56] N. Setoodeh, P. Darvishi, A. Lashanizadegan, Enhancing of asphaltene adsorption onto Fe_3O_4 nanoparticles coated with metal-organic framework Mil-101 (Cr) for the inhibition of asphaltene precipitation, J. Dispersion Sci. Technol., 39 (2017) 452–459.
[57] R.K. Sheshdeh, S. Abbasizadeh, M.R.K. Nikou, K. Badii, M.S. Sharafi, Liquid phase adsorption kinetics and equilibrium of toluene by novel modified-diatomite, J. Environ. Health Sci. Eng., 12 (2014) 148.
[58] N.F. Ahmad, M.A. Kamboh, H.R. Nodeh, S.N.B.A. Halim, S. Mohamad, Synthesis of piperazine functionalized magnetic sporopollenin: a new organic-inorganic hybrid material for the removal of lead (II) and arsenic (III) from aqueous solution, Environ. Sci. Pollut. Res., 24 (2017) 21846–21858.
[59] N. Samadi, R. Hasanzadeh, M. Rasad, Adsorption isotherms, kinetic, and desorption studies on removal of toxic metal ions from aqueous solutions by polymeric adsorbent, J. Appl. Polym. Sci., 132 (2015) 41642–41655.
[60] M.M. Tehrani, S. Abbasizadeh, A. Alamdari, S.E. Mousavi, Prediction of simultaneous sorption of copper (II), cobalt (II) and zinc (II) contaminants from water systems by a novel multi-functionalized zirconia nanofiber, Desal. Wat. Treat., 62 (2017) 403–417.
[61] M. Irani, A.R. Keshtkar, M.A. Mousavian, Removal of Cd (II) and Ni (II) from aqueous solution by PVA/TEOS/TMPTMS hybrid membrane, Chem. Eng. J., 175 (2011) 251–259.
[62] A.A. Wasim, M.N. Khan, Physicochemical effects of alkali treatment on acid-activated pine shell for the removal of lead ions from aqueous medium, J. Dispersion Sci., Technol., 38 (2017) 1092–1102.
[63] C.-C. Liu, M. Kuang-Wang, Y.-S. Li, Removal of nickel from aqueous solution using wine processing waste sludge, Ind. Eng. Chem. Res., 44 (2005) 1438–1445.
[64] K. Zhu, Y. Duan, F. Wang, P. Gao, H. Jia, C. Ma, C. Wang, Silane-modified halloysite/Fe_3O_4 nanocomposites: simultaneous removal of Cr (VI) and Sb (V) and positive effects of Cr (VI) on Sb (V) adsorption, Chem. Eng. J., 311 (2017) 236–246.
[65] E. Metwally, S. Elkholy, H. Salem, M. Elsabee, Sorption behavior of ^{60}Co and $^{152+154}$Eu radionuclides onto chitosan derivatives, Carbohydr. Polym., 76 (2009) 622–631.